

Article

Ternary Planar Heterojunction Organic Solar Cells Based on the Ternary Active Layers: α -6T/AlPcCl/C₆₀

Hajar Ftouhi ^{1,2}, Hind Lamkaouane ², Mustapha Diani ¹, Guy Louarn ^{2,*}, Ludovic Arzel ², Jean-Christian Bernède ³, Mohammed Addou ¹ and Linda Cattin ²

¹ Équipe de Recherche Couches Minces et Nanomatériaux, Faculté des Sciences et Techniques, Université Abdelmalek Essaâdi, BP 416, Tanger 90040, Morocco

² Institut des Matériaux de Nantes Jean Rouxel (IMN), CNRS, Nantes Université, 44000 Nantes, France

³ MOLTECH-Anjou, CNRS, UMR 6200, Nantes Université, 44000 Nantes, France

* Correspondence: guy.louarn@cnrs-imn.fr

Abstract: Ternary planar heterojunction organic solar cells (PHJ-OPVs) were fabricated using three organic small molecules, alpha-sexithiophene (α -6T), aluminum phthalocyanine chloride (AlPcCl) and fullerene (C₆₀). These molecules can be easily sublimated under a vacuum; they have complementary optical absorption spectra and their energy band structure alignment is favorable for electronic charge transfers. Moreover, α -6T and AlPcCl have almost the same HOMO, which is desirable to avoid any decrease in open circuit voltage. The AlPcCl intercalated layer bridges the energy levels of the electron donor, α -6T, and the electron acceptor, C₆₀, which facilitates charge transport through the energy cascade effect. Moreover, the charge carrier mobility measurements of AlPcCl, using the space charge limited current method, demonstrated that it is ambipolar. All these properties combine to improve the power conversion efficiency (PCE) of PHJ-OPVs by moving from binary structures (α -6T/C₆₀, α -6T/AlPcCl and AlPcCl/C₆₀) to ternary ones (α -6T/AlPcCl/C₆₀). We show, in this study, that both interfaces of the ternary PHJ-OPVs are efficient for carrier separation. After optimization of the different layer thickness, we show that, by comparing the optimum efficiencies of the binary PHJ-OPVs, the realization of ternary PHJ-OPVs, based on the active layers α -6T/AlPcCl/C₆₀, using the following optimized method, allows us to achieve a PCE of 4.33%.

Keywords: organic photovoltaic cells; ambipolar organic layer; aluminum phthalocyanine chloride; alpha-sexithiophene



Citation: Ftouhi, H.; Lamkaouane, H.; Diani, M.; Louarn, G.; Arzel, L.; Bernède, J.-C.; Addou, M.; Cattin, L. Ternary Planar Heterojunction Organic Solar Cells Based on the Ternary Active Layers: α -6T/AlPcCl/C₆₀. *Solar* **2022**, *2*, 375–384. <https://doi.org/10.3390/solar2030022>

Academic Editors: Dewei Zhao and Jürgen Heinz Werner

Received: 22 July 2022

Accepted: 5 September 2022

Published: 8 September 2022

Publisher's Note: MDPI stays neutral with regard to jurisdictional claims in published maps and institutional affiliations.



Copyright: © 2022 by the authors. Licensee MDPI, Basel, Switzerland. This article is an open access article distributed under the terms and conditions of the Creative Commons Attribution (CC BY) license (<https://creativecommons.org/licenses/by/4.0/>).

1. Introduction

Different photovoltaic technologies have been developed over the last few decades based on inorganic solar cell technologies, such as crystalline silicon, CdTe, CuInGaSe₂. However, other new technologies are considered to be promising alternatives to participate in solving the energy insecurity problems, for example, photovoltaic cells using perovskite [1], organic photovoltaic cells (OPVs) [2] and hybrid dye-sensitized solar cells (DSSCs) [3]. Among these new technologies, great attention is now being given to organic photovoltaic cells (OPVs), which are supposed to be a very promising alternative or complement due to their distinct properties of low cost, light weight nature, mechanical flexibility, large area coating production and quite simple fabrication techniques [4]. The simplest OPV configuration for the light absorbing layer consists of the use of two superimposed organic layers, the first one being electron donor (D) and the second being the electron acceptor (A). Nevertheless, in order to improve the OPVs' efficiency, other configurations, such as ternary cells, were tested.

Starting from optimized binary OPVs, the use of the ternary strategy has shown great potential in improving OPVs' performances using a well-matched third component [5–7]. In fact, organic semiconductors exhibit quite a narrow absorption band, which results in

limited photon harvesting in classical binary active layers. Using the ternary active layer allows for the widening of the absorption domain using appropriate organic material with complementary absorption spectrum. On the other hand, the energy levels of the three organic semiconductors must be chosen in order to avoid formation of carrier traps at the interfaces of these materials. The third material must bridge the energy levels between the electron donor and the electron acceptor in order to facilitate charge transport through the energy cascade effect. The relative values of the highest occupied molecular orbital (HOMO) and the lowest unoccupied molecular orbital (LUMO) of the organic molecules used must comply with certain conditions. To obtain efficient separation of the exciton charges, the offset Δ_{HOMO} and/or Δ_{LUMO} must be higher than the exciton binding energy Δ_{Exc} [8,9], which corresponds to the minimum offset for charge separation [10–12]. Therefore, in the case of ternary OPVs, HOMO and LUMO energy levels must be progressively offset in the form of cascade heterojunctions, in such a way that the central layer carries out exciton dissociation on the donor and acceptor side, which means that it must be ambipolar (DA). Two typical geometries of the active layer are possible. It may consist of a blend of D and A; this configuration is called bulk heterojunction (BHJ). The second possibility consists of a stacking of layers, where the active layer is made of at least two films, D/A; it is called planar heterojunction (PHJ) [13,14]. In recent times, dramatic advances in the performances of OPVs have been achieved using new promising molecules and polymers [15–17]. Each OPV category has its own advantages and disadvantages. BHJs are known by their high exciton dissociation capability, due to the presence of a large interface area D/A, which reduces the recombination of the excitons. Nevertheless, morphology of the BHJ is difficult to control, which limits the reproducibility of the results [18]. Moreover, over time, there is progressive phase separation and performance degradation [19]. On the other hand, the synthesis of the new no-fullerene materials is not trivial, which means that the commercialization of BHJs panels is not feasible in the near future. Therefore, it is interesting to study the performances of cells using small molecules that are less efficient, but are easier to obtain with perfectly controlled synthesis and reproducible properties [20–22]. The possibility of the deposition of the small molecules under a vacuum allows easy fabrication of multi-layer devices with precise control of the layers' thicknesses [23–25]. Moreover, several small organic molecules have good thermal stability, so they can easily be vacuum deposited as thin films with high purity [26,27].

Therefore, in the present study, we chose to work on ternary PHJ-OPVs (Figure 1). For an active ternary layer such as D/DA/A to be effective, the mobility of carriers of both types, electrons and holes, of DA must be high enough to obtain an acceptable current, i.e., DA must be ambipolar. On the other hand, it is well known that the maximum value of the open circuit voltage, V_{oc} , follows the energy difference between the LUMO of A and the HOMO of D. Therefore, in order to avoid any decrease in V_{oc} , it is desirable to use a DA with similar HOMO (or LUMO) to D (or A).

Considering all these conditions, we have chosen the following three molecules for this study: alpha-sexithiophene (α -6T), aluminum phthalocyanine chloride (AlPcCl) and fullerene (C_{60}) (Figure 1b). In fact, we already optimized binary PHJ-OPVs based on the couples α -6T/ C_{60} , α -6T/AlPcCl and AlPcCl/ C_{60} . If it is known that AlPcCl is an efficient electron donor, we have shown that it can also be successfully used as an electron acceptor; nevertheless, up to the present day, it has not been used as a central ambipolar layer [28]. Moreover, α -6T and AlPcCl have nearly the same HOMO value, while they have complementary absorption domains. Therefore, in the present work, we carried out the study of the ternary PHJ-OPV based on the active layer α -6T/AlPcCl/ C_{60} , using the AlPcCl layer thickness as a parameter. The optimum structure, i.e., α -6T/AlPcCl/ C_{60} , the thicknesses of which are 22 nm/15 nm/45 nm, respectively, allows a power conversion efficiency of more than 4.3%.

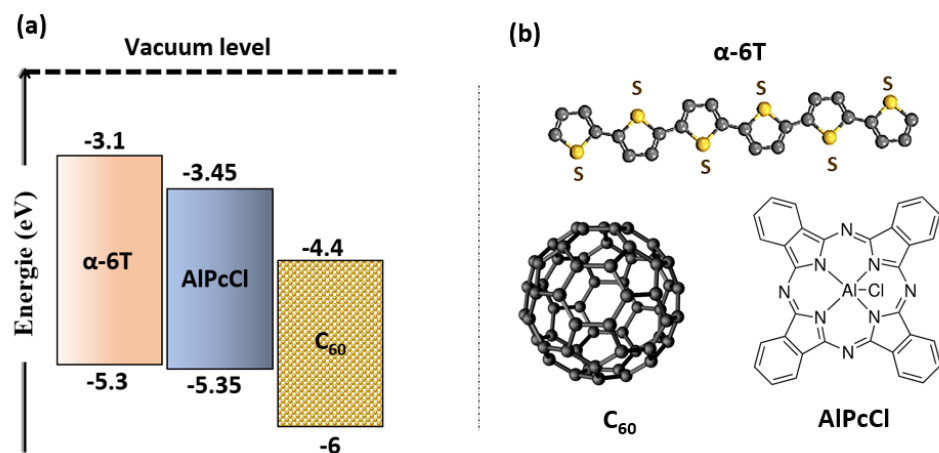


Figure 1. Energy level alignments for the different OPVs (a); small molecules used (b).

2. Materials and Methods

In this work, CODEX France provided the chemical products.

2.1. Realization of the Solar Cells

The multilayer structure of the PHJ-OPVs cell elaborated in this work can be described as follows: ITO/MoO₃/CuI/ α -6T/AlPcCl/C₆₀/Alq3/Al. Here, the substrate was an ITO-coated glass. The hole transporting layer was MoO₃/CuI, where the thickness of MoO₃ and CuI were 3 and 1.5 nm, respectively [29]. The electron transporting layer was Alq3, with a thickness of 9 nm [30]. All these thin layers of our PHJ-OPVs were made in the same run, without breaking the vacuum. All the films were deposited under a vacuum (see below) and the thickness of the films was monitored using a quartz monitor. The deposition process can be summarized as follows: after a classical cleaning process, the ITO-coated glass substrates were rinsed in deionized water, dried under argon flow and loaded into the vacuum chamber of the reactor. All the thin films were then deposited by thermal evaporation under a vacuum (10⁻⁴ Pa). The deposition rates and the thicknesses were measured in situ with a quartz monitor. Based on previous studies, the deposition rates were set at 0.02 nm/s for MoO₃ and 0.05 nm/s for α -6T, AlPcCl, C₆₀ and Alq3. Finally, the aluminum top electrodes were thermally evaporated, without breaking the vacuum, through a mask with 2 mm \times 8 mm active areas.

2.2. Characterizations Techniques

The electrical characteristics of the PHJ-OPVs were measured with an automated I-V tester, in the dark and under sun global AM 1.5 solar illumination. The light intensity of the solar simulator (Oriel 300W) was calibrated at 100 mW/cm², with a PV reference cell (0.5 cm² CIGS solar cell, calibrated at NREL, Golden, CO, USA). The performances of the photovoltaic cells were evaluated in ambient conditions and the devices were illuminated through TCO electrodes. The measurements of incident photon-to-current conversion efficiency were carried out with monochromatic continuous light without modulation. The measurement duration for a given wavelength was long enough to reach a steady-state value and to minimize noise. The external quantum efficiency (EQE) was measured with home-made apparatus. The electron and hole mobilities were measured using the space charge limited current (SCLC) technique. Hole-only devices were based on the following structure: ITO/MoO₃ (3 nm)/CuI (1.5 nm)/D (or DA) (120 nm)/MoO₃ (7 nm)/Al. In the ternary structures, the intercalated layer must be ambipolar to permit the electrons to diffuse. Therefore, we also studied electron-only devices, which were built as follows: ITO/ETL/A (or DA)/ETL/Al. The ETLs (electron transporting layer) were either LiF or Ca. Such layers facilitate electron collection, while they oppose the passage of holes. The probed organic films had a thickness of 100 nm because it must be thick enough to prevent

the interface phenomena that dominate those of bulk. The hole mobility, μ_h , and electron mobility, μ_e , values were calculated using the Mott–Gurney equation [31], which is as follows (Equation (1)):

$$J = 9/8 \epsilon_r \epsilon_0 \mu V^2 / d^3 \quad (1)$$

Here, ϵ_r , the dielectric constant is about 2 for organic semiconducting materials, ϵ_0 is the vacuum permittivity, μ represents the carrier mobility, V represents the applied voltage, and d the active layer thickness. The calculated mobility values were in good agreement with those already published.

Optical absorption spectra were recorded at room temperature, using a UV/visible spectrometer (PERKIN ELMER Lambda 1050 spectrophotometer). The photoluminescence measurements (PL) spectra were recorded using a Fluorolog Jobin-Yvon spectrophotometer. The specimens were illuminated with a 400 nm line of a filtered Xenon lamp (150 W).

3. Results and Discussion

The first part of the study was dedicated to the optimization of the thickness of the three organic layers of the ternary OPV. In fact, the thickness of the α -6T and C₆₀ layers have been already optimized in a binary configuration [32]. Nevertheless, in the preliminary experiments, we studied the effect of the thickness of the D and the A layers, but no improvement in the performances was achieved. Therefore, we focused on the study of the central layer thickness. In Table 1, we can observe that the PHJ-OPV power conversion efficiency increases with the AlPcCl thickness, up to 15 nm. Beyond this optimum, the efficiency starts to decrease. The optimum power conversion efficiency is $\eta = 4.33\%$, which corresponds to an open circuit voltage, V_{oc} , of 0.62 V, a short circuit current, J_{sc} , of 13.90 mA/cm² and a fill factor, FF, of 48%. It can be observed that V_{oc} increases with the increase in AlPcCl thickness. However, if J_{sc} starts increasing with this thickness of AlPcCl, beyond 15 nm it decreases, which results in a decrease in the power conversion efficiency.

Table 1. Parameters of the ternary PHJ-OPVs based on the active layer: 6T/AlPcCl/C₆₀.

Layer Thickness (nm)			V_{oc} (V)	J_{sc} (mA/cm ²)	FF (%)	η (%)
α -6T	AlPcCl	C ₆₀				
22	10	45	0.49	11.70	43	2.50
22	12	45	0.59	11.70	53	3.70
22	13	45	0.61	11.77	43	3.10
22	15	45	0.62	14.60	48	4.33
22	17.5	45	0.63	12.50	47	3.70

The goal of our study on ternary PHJ-OPVs was to surpass the efficiencies obtained with the corresponding binary PHJ-OPVs. Then, after optimizing the performances obtained with the ternary PHJ-OPV 6T/AlPcCl/C₆₀, we compared these results with those due to the couples α -6T/C₆₀, AlPcCl/C₆₀ and α -6T/AlPcCl. The results, obtained after optimization, are presented in Figure 2 and are summarized in Table 2.

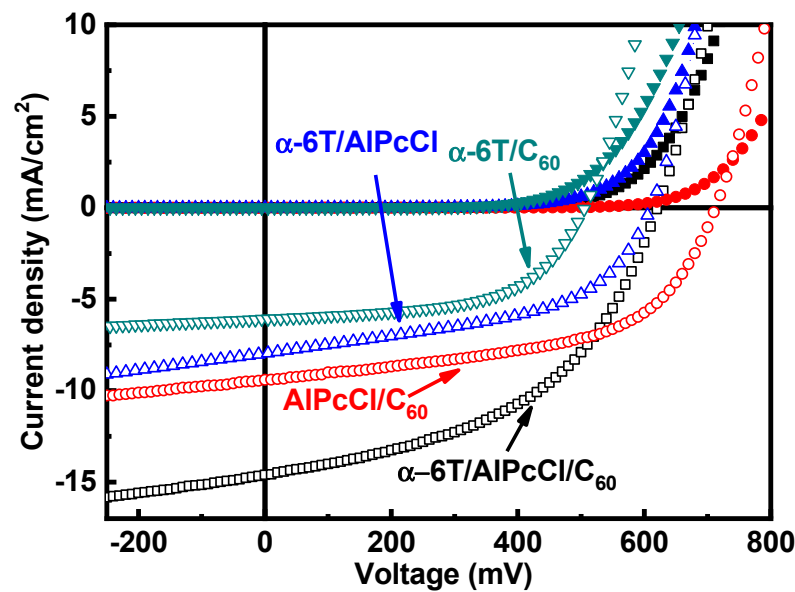


Figure 2. J-V characteristics of binary and ternary PHJ-OPVs: ITO/MoO₃/active layers/Alq₃/Al, the active layer being AIPcCl/C₆₀ (●), α-6T/C₆₀ (▼), α-6T/AIPcCl (▲) and α-6T/AIPcCl/C₆₀ (■), (the filled symbols correspond to dark conditions, while the empty symbols correspond to light AM 1.5 conditions).

Table 2. Parameters of the PHJ-OPV family using α-6T, AIPcCl and C₆₀.

Sample	Thickness (nm)			V _{oc} (V)	J _{sc} (mA/cm ²)	FF (%)	η (%)
	α-6T	AIPcCl	C ₆₀				
α-6T/C ₆₀	22	***	45	0.51	6.10	58	1.77
α-6T/AIPcCl	22	25	***	0.61	7.98	51	2.48
AIPcCl/C ₆₀	***	26	45	0.70	9.61	59.5	3.97
α-6T/AIPcCl/C ₆₀	22	15	45	0.62	14.60	48	4.33

By comparison with binary PHJ-OPVs with α-6T as D, the improvement of the ternary OPV is very significant. Even with the highly performing binary OPVs based on the AIPcCl/C₆₀ couple, there is an increase in the power conversion efficiency. To deepen our understanding of the results, we carried out some complementary experiments. First, we carried out the measurements of the EQE spectra of the different absorbing layers. In Figure 3, the EQE spectra are presented, and it is possible to compare them to the absorbance spectra of the corresponding layers to verify if all the constituents of these different layers were effective in the creation of charge carriers. By comparing the Figures 3 and 4, it is clear that all the EQE spectra follow the absorbance spectra of the corresponding structure. For instance, in the case of the AIPcCl/C₆₀ active bilayer, the shape of the EQE spectrum follows that of the absorption spectrum of AIPcCl, with a clear contribution of C₆₀ for wavelengths below 500 nm. In the case of α-6T/C₆₀, the EQE spectrum exhibits a prominent peak with a maximum around λ = 460 nm (Figure 3), while the absorption maximum of α-6T is situated at λ = 410 nm (Figure 4). The slight red-shift of the EQE spectrum is due to some contribution of the C₆₀ layer and the absorption curve exhibits a shoulder at around 460 nm. In the case of the α-6T/AIPcCl couple, the contributions of α-6T and AIPcCl are clearly visible in both spectra (Figures 3 and 4). The first EQE maximum appears at λ = 740 nm, which can be attributed to the excitons issued from AIPcCl, while the second broad peak, situated between λ = 350 nm and 550 nm, must be mainly attributed to α-6T, as shown by their absorption spectra.

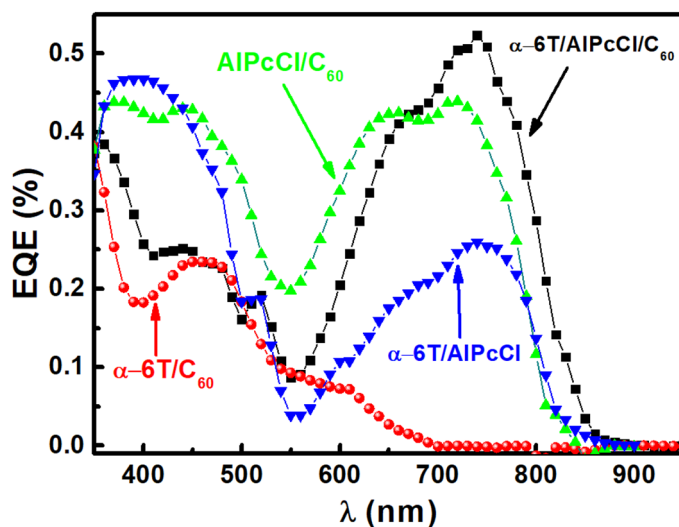


Figure 3. EQE spectra of PHJ-OPVs with different active layers: (■) α -6T/AIPcCl/ C_{60} , (▲) AIPcCl/ C_{60} , (▼) α -6T/AIPcCl and (●) α -6T/ C_{60} .

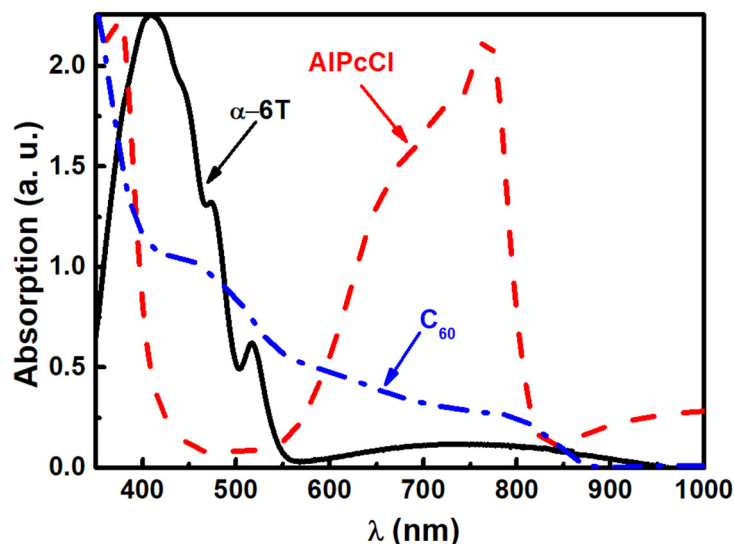


Figure 4. Absorbance spectra of α -6T (—), AIPcCl (---) and C_{60} (---).

Therefore, the EQE curve of the α -6T/AIPcCl structures demonstrates that both layers are clearly active. Finally, both interfaces of the α -6T/AIPcCl/ C_{60} ternary structure are active, as shown in Figure 3; the shape of the EQE spectrum of the ternary PHJ-OPV follows that of the optical absorbance (Figure 4). The band gaps of the donors AIPcCl and α -6T can be calculated from the absorbance spectra presented in Figure 4. The estimated value for AIPcCl is 1.51 eV, which is in good agreement with the value reported in the literature [33]. Concerning the band gap of α -6T, the value estimated from the absorbance spectrum is 2.2 eV, while that calculated from the PL graph [34] is 2.35 eV. These values are in good agreement, given the experimental uncertainties (± 0.5 eV) concerning these measurements.

In Table 2, we can observe that the J_{sc} value of the ternary PHJ-OPV is significantly higher than those of the binary PHJ-OPVs. Such an improvement can be attributed to different contributions. First, the absorbance range of the active layer is far broader than those of the binary OPVs with C_{60} as the acceptor, which permits a broader spectral response. Second, J_{sc} depends not only on the number of created excitons but also on the charge generation efficiency. We have observed that both interfaces in the ternary α -

6T/AIPcCl/C₆₀ PHJ-OPVs are efficient, which contributes significantly to the increase in J_{sc}. In addition to the classical charge generation at the interface ED/EA through the classical four steps process (a/absorption of light and exciton generation, b/exciton diffusion to an interface D/A, c/exciton dissociation and charge carrier generation at the interface, d/charge carrier collection at the electrodes), there is an alternative possible migration, through energy transfer. It corresponds to a two-step process, which first includes the diffusion of the exciton from D to the central ambipolar layer, DA, over long-distance scales, followed by dissociation. This diffusion over long distances occurs due to a type of energy transfer named “Föster resonance energy transfer-FRET”. Therefore, this FRET process is likely to initiate the two-step exciton dissociation process, which first includes large-scale FRET exciton diffusion from D to DA, and then dissociation at the DA/A interface. However, the FRET process, to be efficient, needs overlapping between the D emission spectrum and the DA absorption spectrum [35–37]. In the present case, the absorption spectrum of AIPcCl exhibits two main features, one band between 550 nm and 800 nm and the other one in the UV range from 400 nm and less (Figure 4). On the other hand, α-6T presents a strong emission peak between 500 nm and 750 nm, as shown in Figure 5. It means that Föster resonance energy transfer-FRET is highly probable in the ternary PHJ-OPVs based on α-6T/AIPcCl/C₆₀. Indeed, when the α-6T layer is covered with a thin AIPcCl (15 nm) layer, the photoluminescence signal decreases significantly (Figure 5). The high efficiency of the AIPcCl quenching layer indicates that the FRET from α-6T to AIPcCl is very efficient [25].

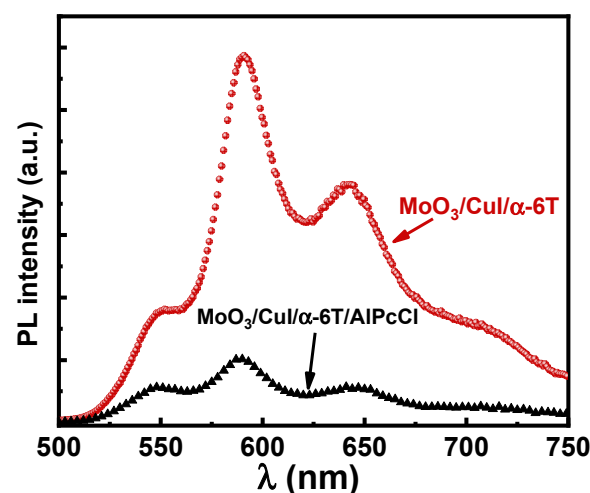


Figure 5. Photoluminescence spectrum of a α-6T layer alone (●) and covered by AIPcCl (▲).

At room temperature, the emission spectra of α-6T consists of three bands located at 2.25 eV, 2.10 eV, and 1.92 eV, which is in excellent agreement with the literature [38]. The most energetic emission peak, located at 2.25 eV, is identified as the 0-0 excitonic transition, which is located at 2.27 eV; the others are generally attributed to vibronic coupling.

We also carried out the carrier mobility measurements of the different organic layers. Thus, electron and hole mobilities of AIPcCl have been estimated using the SCLC method (see “Materials and Methods” section). The values obtained are $\mu_e = 6.9 \times 10^{-4} \text{ cm}^2/\text{Vs}$ and $\mu_h = 4 \times 10^{-5} \text{ cm}^2/\text{Vs}$. The electron mobility of C₆₀ is $\mu_e = 1.5 \times 10^{-2} \text{ cm}^2/\text{Vs}$, which is an acceptable value for an amorphous layer [39].

On the other hand, it is well accepted that, if nearly ohmic contacts between organic layers and electrodes are realized, V_{oc} is directly related to the difference between LUMO_A and HOMO_D according to the following Equation (2):

$$qV_{oc} = \text{LUMO}_A - \text{HOMO}_D - \Delta \quad (2)$$

The Δ value depends on recombination losses, which depend on the D/A interface quality [40]. The different LUMO_A-HOMO_D values for α -6T/C₆₀, AlPcCl/C₆₀ and α -6T/AlPcCl are 0.9 eV, 0.95 eV and 1.85 eV, respectively. Therefore, if the tendency given by Equation (1) is corroborated by the results presented in Table 2, it must be noted that for the couple α -6T/AlPcCl, the Voc value is far from the maximum theoretical value. It means that, if the interface α -6T/AlPcCl is efficient, it is not as efficient as the α -6T/C₆₀ and AlPcCl/C₆₀ interfaces. Such a limitation of the efficiency of AlPcCl as an acceptor can be attributed to the fact that the electron mobility of AlPcCl, $\mu_{e(\text{AlPcCl})} = 6.9 \times 10^{-4} \text{ cm}^2/\text{Vs}$, is significantly smaller than that encountered in C₆₀ ($\mu_{e(\text{C60})} = 1.5 \times 10^{-2} \text{ cm}^2/\text{Vs}$.) This hypothesis is supported by the smaller FF values obtained when AlPcCl was used as an acceptor. In the case of the ternary structure, Voc is only slightly higher than that of the junction α -6T/C₆₀, which means that, as expected, the Voc value is limited by the difference between the LUMO of C₆₀ and the HOMO of α -6T. Nevertheless, as shown in Table 2, by comparison with the best results obtained with binary OPVs, the ternary α -6T/AlPcCl/C₆₀ PHJ-OPV permits an improvement in the power conversion efficiency.

Finally, it is well known that bulk and interfacial morphology play an important role in charge generation, recombination, and extraction in OPVs [41]. Therefore, we carried out SEM and AFM studies at each stage of cell development. Firstly, as shown previously [32], α -6T deposited on the hybrid HTL layer MoO₃/CuI has a monoclinic polycrystalline structure. This crystallization induces a strong increase in thin film absorption, which contributes to an important increase in the Jsc of the cells using the hybrid HTL layer MoO₃/CuI. XRD patterns of the AlPcCl and C₆₀ layers show that these films are amorphous. The AFM study shows that α -6T layers consist of small grains that are distributed homogeneously over the entire sample area, with an RMS (root mean square roughness) of about 2.7 nm. This low roughness limits the leakage currents present when the surface roughness is too high. When deposited onto ITO/MoO₃/CuI/ α -6T, the AlPcCl surface has a continuous texture formed by «stems», which are distributed randomly, leading to a surface roughness of 12.3 nm [28]. After deposition of the C₆₀ layer (45 nm thick), it is observed that it has a homogeneous and continuous texture formed by features with diameters around 100 nm, which are distributed randomly. This leads to an RMS roughness smaller than 10 nm. As a result, the leakage current is lower (unpublished results), which contributes to the higher performance of the ternary cells.

4. Conclusions

In order to overcome the disadvantage of binary OPVs due to their narrow absorption spectrum, it is possible to use ternary OPVs with constituent layers of complementary absorption domains. During this work, we have chosen α -6T as the electron donor, C₆₀ as the electron acceptor and AlPcCl as the ambipolar layer. Indeed, we had already shown that AlPcCl can be used as an acceptor layer in binary OPVs [28]. Depending on the organic materials chosen to build the active layer, different models can be used to describe the operating mechanism of ternary OPVs, which are as follows: (i) the classical charge transfer via the four-step process, (ii) the parallel mechanism of which the ternary structure behaves as if it was two diodes in parallel [42], (iii) the formation of an interpenetrating bulk heterojunction structure, which is possible when there is a high degree of compatibility between the donor and the acceptor materials [43], and, finally, (iv) the energy transfer mechanism by Förster resonance energy transfer (FRET) [35–37].

In the present work, the studied devices were PHJ-OPVs, in which the different organic thin films were stacked and continuous. We also showed that charge transfer and energy transfer mechanisms operate simultaneously in the ternary α -6T/AlPcCl/C₆₀ devices, which justifies the significant improvement of the power conversion efficiency of the ternary PHJ-OPVs, compared to the corresponding binary PHJ-OPVs. Nevertheless, the optimum efficiency remains quite low, which may be attributed to the low value of the Voc. The theoretical maximum value of Voc as LUMO_A-HOMO_D was 0.9 eV, which prompts the study of this OPV system using an electron donor with a HOMO absolute value higher than 5.6 eV, which would correspond to a Voc value of 1.2 eV.

Author Contributions: Conceptualization, H.F. and J.-C.B.; methodology, L.C. and L.A.; software, G.L.; validation, L.C., G.L. and J.-C.B.; formal analysis, H.F. and M.D.; investigation, H.F. and H.L.; data curation, G.L.; writing—original draft preparation, H.F. and J.-C.B.; writing—review and editing, H.F., G.L. and J.-C.B.; supervision, M.A. and L.C. All authors have read and agreed to the published version of the manuscript.

Funding: The Hubert Curien program (PHC), under the french-moroccan grant agreements (TOUBKAL) No. 41406ZC.

Institutional Review Board Statement: Not applicable.

Informed Consent Statement: Not applicable.

Data Availability Statement: Not available.

Acknowledgments: We gratefully acknowledge «le Centre National de la Recherche Scientifique et Technique (CNRS)» (PPR/2015/9—Ministère Marocain), le Partenariat Hubert Curien (PHC) franco-marocain TOUBKAL, project under contract No. 41406ZC.

Conflicts of Interest: The authors declare no conflict of interest.

References

1. Bouich, A.; Marí-Guaita, J.; Sahraoui, B.; Palacios, P.; Mari1, B. Tetrabutylammonium (TBA)-Doped Methylammonium Lead Iodide: High Quality and Stable Perovskite Thin Films. *Front. Energy Res.* **2022**, *10*, 840817. [[CrossRef](#)]
2. Sampaio, P.G.V.; González, M.O.A. A review on organic photovoltaic cell. *Int. J. Energy Res.* **2022**. [[CrossRef](#)]
3. Chang, D.W.; Choi, H.J.; Filer, A.; Baek, J.B. Graphene in photovoltaic applications: Organic photovoltaic cells (OPVs) and dye-sensitized solar cells (DSSCs). *J. Mater. Chem. A* **2014**, *2*, 12136–12149. [[CrossRef](#)]
4. Hains, A.W.; Liang, Z.; Woodhouse, M.A.; Gregg, B.A. Molecular semiconductors in organic photovoltaic cells. *Chem. Rev.* **2010**, *110*, 6689–6735. [[CrossRef](#)] [[PubMed](#)]
5. Wang, X.; Sun, Q.; Gao, J.; Ma, X.; Son, J.H.; Jeong, S.Y.; Hu, Z.; Niu, L.; Woo, H.Y.; Zhang, J.; et al. Ternary Organic Photovoltaic Cells Exhibiting 17.59% Efficiency with Two Compatible Y6 Derivations as Acceptor. *Solar Rrl* **2021**, *5*, 2100007. [[CrossRef](#)]
6. Ma, X.; Zeng, A.; Gao, J.; Hu, Z.; Xu, C.; Son, J.H.; Jeong, S.Y.; Zhang, C.; Li, M.; Wang, K.; et al. Approaching 18% efficiency of ternary organic photovoltaics with wide bandgap polymer donor and well compatible Y6: Y6-1O as acceptor. *Natl. Sci. Rev.* **2021**, *8*, nwaa305. [[CrossRef](#)]
7. Ram, K.S.; Singh, J. Over 20% Efficient and Stable Non-Fullerene-Based Ternary Bulk-Heterojunction Organic Solar Cell with WS₂ Hole-Transport Layer and Graded Refractive Index Antireflection Coating. *Adv. Theory Simul.* **2020**, *3*, 2000047. [[CrossRef](#)]
8. Gong, X.; Tong, M.; Brunetti, F.G.; Seo, J.; Sun, Y.; Moses, D.; Wudl, F.; Heeger, A.J. Bulk Heterojunction Solar Cells with Large Open-Circuit Voltage: Electron Transfer with Small Donor-Acceptor Energy Offset. *Adv. Mater.* **2011**, *23*, 2272–2277. [[CrossRef](#)] [[PubMed](#)]
9. Baran, D.; Kirchartz, T.; Wheeler, S.; Dimitrov, S.; Abdelsamie, M.; Gorman, J.; Ashraf, R.S.; Holliday, S.; Wadsworth, A.; Gasparini, N.; et al. Reduced voltage losses yield 10% efficient fullerene free organic solar cells with >1 V open circuit voltages. *Energy Environ. Sci.* **2016**, *9*, 3783. [[CrossRef](#)]
10. Bin, H.; Zhang, Z.-G.; Gao, L.; Chen, S.; Zhong, L.; Xue, L.; Yang, C.; Li, Y. Non-Fullerene Polymer Solar Cells Based on Alkylthio and Fluorine Substituted 2D-Conjugated Polymers Reach 9.5% Efficiency. *J. Am. Chem. Soc.* **2016**, *138*, 4657–4664. [[CrossRef](#)] [[PubMed](#)]
11. Narayan, M.; Singh, J. Study of the mechanism and rate of exciton dissociation at the donor-acceptor interface in bulk-heterojunction organic solar cells. *J. Appl. Phys.* **2013**, *114*, 073510. [[CrossRef](#)]
12. Singh, J.; Narayan, M.; Ompong, D.; Zhu, F. Dissociation of charge transfer excitons at the donor–acceptor interface in bulk heterojunction organic solar cells. *J. Mater. Sci. Mater. Electron.* **2017**, *28*, 7095–7099. [[CrossRef](#)]
13. Lorch, C.; Barnajee, R.; Dieterle, J.; Hinderhofer, A.; Gerlach, A.; Drnec, J.; Schreiber, F. Templating effects of a-sexithiophene in donor-acceptor organic thin films. *J. Phys. Chem. C* **2015**, *119*, 23211–23220. [[CrossRef](#)]
14. Bernède, J.C. Organic photovoltaic cells: History, principle and techniques. *J. Chil. Chem. Soc.* **2008**, *53*, 1549–1564. [[CrossRef](#)]
15. Gao, F. A New Acceptor for Highly Efficient Organic Solar Cells. *Joule* **2019**, *3*, 908–919. [[CrossRef](#)]
16. Zhang, G.; Zhao, J.; Chow, P.C.Y.; Jiang, K.; Zhang, J.; Zhu, Z.; Zhang, J.; Huang, F.; Yan, H. Nonfullerene Acceptor Molecules for Bulk Heterojunction Organic Solar Cells. *Chem. Rev.* **2018**, *118*, 3447–3507. [[CrossRef](#)] [[PubMed](#)]
17. Liu, Q.; Jiang, Y.; Jin, K.; Qin, J.; Xu, J.; Li, W.; Xiona, J.; Liu, J.; Xiao, Z.; Sun, K.; et al. 18% efficiency organic solar cells. *Sci. Commun.* **2020**, *65*, 272–275. [[CrossRef](#)]
18. Yang, W.; Luo, Y.; Guo, P.; Sun, H.; Yao, Y. Leakage Current Induced by Energetic Disorder in Organic Bulk Heterojunction Solar Cells: Comprehending the Ultrahigh Loss of Open-Circuit Voltage at Low Temperatures. *Phys. Rev. Appl.* **2017**, *7*, 044017. [[CrossRef](#)]
19. Schaffer, C.J.; Palumbiny, C.M.; Niedermeier, M.A.; Jendrzewski, C.; Santoro, G.; Roth, S.V.; Müller-Buschbaum, P. A Direct Evidence of Morphological Degradation on a Nanometer Scale in Polymer Solar Cells. *Adv. Mater.* **2013**, *25*, 6760–6764. [[CrossRef](#)]

20. Wang, K.; Song, X.; Guo, X.; Wang, Y.; Lai, X.; Meng, F.; Du, M.; Fan, D.; Zhang, R.; Li, G.; et al. Efficient as-cast thick film small-molecule organic solar cell with less fluorination on the donor. *Mater. Chem. Front.* **2020**, *4*, 206. [[CrossRef](#)]
21. He, X.; Yin, L.; Li, Y. Design of organic small molecules for photovoltaic application with high open-circuit voltage (Voc). *J. Mater. Chem. C* **2019**, *7*, 2487–2521. [[CrossRef](#)]
22. Po, R.; Roncali, J. Beyond efficiency: Scalability of molecular donor materials for organic photovoltaics. *Mater. Chem. C* **2016**, *4*, 3677–3685. [[CrossRef](#)]
23. Zhang, Q.; Kan, B.; Liu, F.; Long, G.; Wan, X.; Chen, X.; Zuo, Y.; Ni, W.; Zhang, H.; Li, M.; et al. Small-molecule solar cells with efficiency over 9%. *Nat. Photonics* **2015**, *9*, 35–41. [[CrossRef](#)]
24. Galindo, S.; Ahmadpour, M.; Gerling, L.G.; Marsal, A.; Voz, C.; Alcubilla, R.; Puigdollers, J. Influence of the density of states on the open-circuit voltage in small-molecule solar cells. *Org. Electron.* **2014**, *15*, 2553–2560. [[CrossRef](#)]
25. Cnops, K.; Rand, B.P.; Cheyng, D.; Verreert, B.; Empl, M.A.; Heremans, P. 8.4% efficient fullerene-free organic solar cells exploiting long-range exciton energy transfer. *Nat. Commun.* **2014**, *5*, 3406. [[CrossRef](#)]
26. Leliège, A.; Grolleau, J.; Allain, M.; Blanchard, P.; Demeter, D.; Rousseau, T.; Roncali, J. Small D-p-A systems with s-phenylenebridged accepting units as active materials for organic photovoltaics. *Chem.—Eur. J.* **2013**, *19*, 9948–9960. [[CrossRef](#)] [[PubMed](#)]
27. Ilmin, R.; Haque, A.; Khan, M.S. High efficiency small molecule based donor materials for organic solar cells. *Org. Electron.* **2018**, *58*, 53–62. [[CrossRef](#)]
28. Ftouhi, H.; Lamkaouane, H.; Louarn, G.; Diani, M.; Bernède, J.-C.; Addou, M.; Ftouhi, H.; Lamkaouane, H.; Louarn, G.; Diani, M.; et al. Investigation of aluminum phthalocyanine chloride as acceptor material in planar organic solar cells: Comparative study with fullerene. *J. Mater. Sci. Mater. Electron.* **2021**, *32*, 27710–27720. [[CrossRef](#)]
29. El Jouad, Z.; Morsli, M.; Louarn, G.; Cattin, L.; Addou, M.; Bernède, J.-C. Improving the efficiency of subphthalocyanine based planar organic solar cells through the use of MoO₃/CuI double anode buffer layer. *Sol. Energy Mater. Sol. Cells* **2015**, *141*, 429–435. [[CrossRef](#)]
30. Lakhdar Toumi, A.; Khelil, A.; Tobel, K.; Makha, M.; Hernández, L.A.; Mouchaal, Y.; Cattin, L.; del Valle, M.A.; Diaz, F.R.; Bernède, J.-C. On the exciton blocking layer at the interface organic/cathode in planar multiheterojunction organic solar cells. *Solid State Electron.* **2015**, *104*, 1–5. [[CrossRef](#)]
31. Qin, P.; Fang, G.; Zeng, W.; Fan, X.; Zheng, Q.; Cheng, F.; Wan, J.; Zhao, X. Influence of thermal radiation during aluminium thermal evaporation on organic solar cells. *Sol. Energy Mater. Sol. Cells* **2011**, *95*, 3311. [[CrossRef](#)]
32. Ftouhi, H.; El-Menyawy, E.M.; Lamkaouane, H.; Diani, M.; Louarn, G.; Bernède, J.-C.; Addou, M.; Cattin, L. Efficient planar heterojunction based on α -sexithiophene/fullerene through the use of MoO₃/CuI anode buffer layer. *Thin Solid Films* **2022**, *41*, 139025. [[CrossRef](#)]
33. Ballarotto, M.; Herman, W.N.; Romero, D.B. Low-bandgap small molecules for near-infrared photovoltaic applications. *J. Photonics Energy* **2011**, *1*, 011102. [[CrossRef](#)]
34. Mari-Guaita, J.; Bouich, A.; Mari, B. Shedding Light on Phase Stability and Surface Engineering of Formamidinium Lead Iodide (FAPbI₃) Thin Films for Solar Cells. *Eng. Proc.* **2021**, *12*, 1. [[CrossRef](#)]
35. Liu, D.; Fan, P.; Zhang, D.; Zhang, X.; Yu, J. Förster resonance energy transfer and improved charge mobility for high performance and low-cost ternary polymer solar cells. *Sol. Energy* **2019**, *189*, 186–193. [[CrossRef](#)]
36. Coffey, D.C.; Ferguson, A.J.; Kopidakis, N.; Rumbles, G. Photovoltaic charge generation in organic semiconductors based on long-range energy transfer. *ACS Nano* **2010**, *4*, 5437–5445. [[CrossRef](#)] [[PubMed](#)]
37. Singh, J.; Narayan, M.R.; Ompong, D. Comparative contributions of singlet and triplet excitons in the performance of organic devices. *Phys. Status Solidi* **2016**, *13*, 77–80. [[CrossRef](#)]
38. Mani, A.; Schoonman, J.; Goossens, A. Photoluminescence study of sexithiophene thin films. *J. Phys. Chem. B* **2005**, *109*, 4829–4836. [[CrossRef](#)]
39. Mendil, N.; Daoudi, M.; Berkai, Z.; Belghachi, A. Disorder effect on carrier mobility in Fullerene organic semiconductor. *J. Phys. Conf. Ser.* **2015**, *647*, 012057. [[CrossRef](#)]
40. Benduhn, J.; Tvingstedt, K.; Piersimoni, F.; Ullbrich, S.; Fan, Y.; Tropiano, M.; McGarry, K.A.; Zeika, O.; Riede, M.K.; Douglas, C.J.; et al. Intrinsic non-radiative voltage losses in fullerene-based organic solar cells. *Nat. Energy* **2017**, *2*, 17053. [[CrossRef](#)]
41. Karki, A.; Vollbrecht, J.; Gillett, A.J.; Xiao, S.S.; Yang, Y.; Peng, Z.; Schopp, N.; Dixon, A.L.; Yoon, S.; Schrock, M.; et al. The role of bulk and interfacial morphology in charge generation, recombination, and extraction in non-fullerene acceptor organic solar cells. *Energy Environ. Sci.* **2020**, *13*, 3679–3692. [[CrossRef](#)]
42. Cattin, L.; El Jouad, Z.; Siad, M.B.; Mohammed Krarroubi, A.; Neculqueo, G.; Arzel, L.; Stephant, N.; Mastropasqua Talamo, M.; Martinez, F.; Addou, M.; et al. Highlighting the possibility of parallel mechanism in planar ternary photovoltaic cells. *AIP Adv.* **2018**, *8*, 115329. [[CrossRef](#)]
43. Zhan, L.; Li, S.; Lau, T.K.; Cui, Y.; Lu, X.; Shi, M.; Li, C.Z.; Li, H.; Hou, J.; Chen, H. Over 17% efficiency ternary organic solar cells enabled by two non-fullerene acceptors working in an alloy-like model. *Energy Environ. Sci.* **2020**, *13*, 635–645. [[CrossRef](#)]